

responses of some A1 cells to species-specific vocalizations²⁹ or to combinations of different sounds³⁰ may be well suited for processing certain attributes of natural sound sources. □

Methods

Spatial receptive field measurement

Extracellular recordings were performed in A1 of barbiturate anaesthetized ferrets, using standard techniques²². VAS stimuli for SRF recording were 20-ms gaussian noise bursts convolved with finite impulse response filters that mimicked the direction-dependent frequency transfer characteristics of the head and outer ears. The filters were based on acoustical recordings obtained from each individual animal before the electrophysiological recording sessions. Stimulus presentations from 224 virtual source directions were randomly interleaved. Responses were averaged over five stimulus presentations for each virtual direction. Continuous SRF maps were generated from the averaged responses by triangulation and smoothing with a 45° wide running average filter. SRF maps are shown here using a quartic-azimuthal equal area map projection. See ref. 22 for further details.

Frequency-time response field measurement

Binaural FTRFs were determined by reverse correlation to random chord sequence stimuli similar to those introduced in ref. 16. Twenty-millisecond tone pips (5-ms rise/fall time) were started randomly at any of 60 frequency bands that spanned 0.5 to 32 kHz in a tenth of an octave steps. The probability of a tone pip starting in any one frequency band during any 5-ms time interval was set to values between 1 and 2%, so that, on average, 2.4 to 4.8 tone pips would be on simultaneously at any time during the random chord sequence. Tone onsets in different frequency bands and subsequent time intervals were statistically independent. Two statistically independent random chord sequences were presented simultaneously, one to each ear. Binaural FTRFs were determined by spike-triggered averaging of peri-spike random chord sequence segments. Binaural FTRFs were typically based on 500 to 1,500 spikes, which took between 15–20 min to collect. Determined in this way, FTRFs are usually interpreted as posterior probability distributions for the presence of a tonal stimulus in a particular frequency band and ear and at a particular time in the past, given that a spike was observed at time zero. To generate response predictions we use a converse interpretation, namely that the FTRF estimates a change in mean firing rate at a particular latency if acoustic energy is applied to a particular frequency band. Inherent in this interpretation is the assumption that the response of A1 neurons is adequately approximated as a sum of acoustic energies, weighted and delayed by frequency band according to the FTRF.

Sound levels

Stimulus levels in these experiments were chosen arbitrarily, and varied from unit to unit. Our primary concern was to make good use of the available dynamic range of the digital signal processing equipment, and no attempt was made to match the sound levels of the VAS stimuli used to map the SRFs to the sound levels of the random chord sequences used to estimate the binaural FTRFs. In fact, matching the levels of these very different types of auditory stimuli would pose difficult technical problems. However, to allow a post hoc comparison between the sound levels used during the FTRF measurement and the SRF mapping we estimated the level of the VAS stimuli within the excitatory frequency bands revealed by the FTRF. These values are given as FTRF-weighted VAS levels (in dB relative to 20 µPa) in the figure legends, and give the average energy of the VAS stimuli weighted by a normalized frequency contour through the maximum of the binaural FTRF at the virtual sound direction where this value is greatest. Also stated is the approximate level of the VAS stimuli relative to the unit threshold (estimated by presenting VAS stimuli at varying attenuations) and the sound level of a single tonal component of the reverse correlation stimuli used to determine the binaural FTRF (the single tonal revcor component). In our data set, FTRF-weighted VAS levels varied from 0 to 90 dB SPL, while tonal revcor component levels varied from 30 to 70 dB SPL. VAS and revcor levels were uncorrelated, and over the range of levels tested, the quality of the linear predictions was independent of sound levels.

Received 25 May; accepted 7 September 2001.

- King, A. J., Schnupp, J. W. H. & Doubell, T. P. The shape of ears to come: dynamic coding of auditory space. *Trends Cogn. Sci.* **5**, 261–270 (2001).
- Jenkins, W. M. & Merzenich, M. M. Role of cat primary auditory cortex for sound-localization behavior. *J. Neurophysiol.* **52**, 819–847 (1984).
- Kavanagh, G. L. & Kelly, J. B. Contribution of auditory cortex to sound localization by the ferret (*Mustela putorius*). *J. Neurophysiol.* **57**, 1746–1766 (1987).
- Masterton, R. B. in *Acoustical Signal Processing in the Central Auditory System* (ed. Syka, J.) 1–17 (Plenum, New York, 1997).
- Hefner, H. E. & Hefner, R. S. Effect of bilateral auditory cortex lesions on sound localization in Japanese macaques. *J. Neurophysiol.* **64**, 915–931 (1990).
- Goldberg, J. M. & Brown, P. B. Response of binaural neurons of dog superior olivary complex to dichotic tonal stimuli: some physiological mechanisms of sound localisation. *J. Neurophysiol.* **32**, 613–636 (1969).
- Kitzes, L. M., Wrege, K. S. & Cassady, J. M. Patterns of responses of cortical cells to binaural stimulation. *J. Comp. Neurol.* **192**, 455–472 (1980).
- Yu, J. J. & Young, E. D. Linear and nonlinear pathways of spectral information transmission in the cochlear nucleus. *Proc. Natl Acad. Sci. USA* **97**, 11780–11786 (2000).
- Peña, J. L. & Konishi, M. Auditory spatial receptive fields created by multiplication. *Science* **292**, 249–252 (2001).
- Tian, B., Reser, D., Durham, A., Kustov, A. & Rauschecker, J. P. Functional specialization in rhesus monkey auditory cortex. *Science* **292**, 290–293 (2001).

- Recanzone, G. H., Guard, D. C., Phan, M. L. & Su, T. K. Correlation between the activity of single auditory cortical neurons and sound-localization behavior in the macaque monkey. *J. Neurophysiol.* **83**, 2723–2739 (2000).
- Wightman, F. L. & Kistler, D. J. in *Human Psychophysics* (eds Yost, W. A., Popper, A. N. & Fay, R. R.) 155–192 (Springer, New York, 1993).
- Hofman, P. M. & Van Opstal, A. J. Spectro-temporal factors in two-dimensional human sound localization. *J. Acoust. Soc. Am.* **103**, 2634–2648 (1998).
- Wightman, F. L. & Kistler, D. J. Monaural sound localization revisited. *J. Acoust. Soc. Am.* **101**, 1050–1063 (1997).
- Clarke, S., Bellmann, A., Meuli, R. A., Assal, G. & Steck, A. J. Auditory agnosia and auditory spatial deficits following left hemispheric lesions: evidence for distinct processing pathways. *Neuropsychologia* **38**, 797–807 (2000).
- deCharms, R. C., Blake, D. T. & Merzenich, M. M. Optimizing sound features for cortical neurons. *Science* **280**, 1439–1443 (1998).
- Kowalski, N., Depireux, D. A. & Shamma, S. A. Analysis of dynamic spectra in ferret primary auditory cortex. II. Prediction of unit responses to arbitrary dynamic spectra. *J. Neurophysiol.* **76**, 3524–3534 (1996).
- Movshon, J. A., Thompson, I. D. & Tolhurst, D. J. Spatial summation in the receptive fields of simple cells in the cat's striate cortex. *J. Physiol. Lond.* **283**, 53–77 (1978).
- Phillips, D. P., Judge, P. W. & Kelly, J. B. Primary auditory cortex in the ferret (*Mustela putorius*): neural response properties and topographic organization. *Brain Res.* **443**, 281–294 (1988).
- Carlike, S. The auditory periphery of the ferret. II: The spectral transformations of the external ear and their implications for sound localization. *J. Acoust. Soc. Am.* **88**, 2196–2204 (1990).
- Clarey, J. C., Barone, P. & Imig, T. J. in *The Mammalian Auditory Pathway: Neurophysiology* (eds Popper, A. & Fay, R.) 232–334 (Springer, New York, 1992).
- Mrsic-Flogel, T. D., King, A. J., Jenison, R. L. & Schnupp, J. W. H. Listening through different ears alters spatial response fields in ferret primary auditory cortex. *J. Neurophysiol.* **86**, 1043–1046 (2001).
- Brugge, J. F. et al. Simulation of free-field sound sources and its application to studies of cortical mechanisms of sound localization in the cat. *Hear. Res.* **73**, 67–84 (1994).
- Middlebrooks, J. C. & Pettigrew, J. D. Functional classes of neurons in primary auditory cortex of the cat distinguished by sensitivity to sound location. *J. Neurosci.* **1**, 107–120 (1981).
- Samson, F. K., Barone, P., Clarey, J. C. & Imig, T. J. Effects of ear plugging on single-unit azimuth sensitivity in cat primary auditory cortex. II. Azimuth tuning dependent upon binaural stimulation. *J. Neurophysiol.* **71**, 2194–2216 (1994).
- Ruggero, M. A. in *The Mammalian Auditory Pathway: Neurophysiology* (eds Popper, A. N. & Fay, R. R.) 34–93 (Springer, New York, 1992).
- Schreiner, C. E. Spatial distribution of responses to simple and complex sounds in the primary auditory cortex. *Adiol. Neurootol.* **3**, 104–122 (1998).
- Read, H. L., Winer, J. A. & Schreiner, C. E. Modular organization of intrinsic connections associated with spectral tuning in cat auditory cortex. *Proc. Natl Acad. Sci. USA* **98**, 8042–8047 (2001).
- Wang, X. On cortical coding of vocal communication sounds in primates. *Proc. Natl Acad. Sci. USA* **97**, 11843–11849 (2000).
- Nelken, I., Rotman, Y. & Bar Yosef, O. Responses of auditory-cortex neurons to structural features of natural sounds. *Nature* **397**, 154–157 (1999).

Acknowledgements

We are grateful to D. Moore and A. Parker for comments on an earlier draft of this manuscript. This work was supported by Defeating Deafness (Dunhill Research Fellowship to J.W.H.S.) and by the Wellcome Trust (Wellcome Prize Studentship to T.D.M.F. and Wellcome Senior Research Fellowship to A.J.K.).

Correspondence and requests for materials should be addressed to J.W.H.S. (e-mail: jan.schnupp@physiol.ox.ac.uk).

Target neuron prespecification in the olfactory map of *Drosophila*

Gregory S. X. E. Jefferis*†‡, Elizabeth C. Marin†‡, Reinhard F. Stocker§ & Liqun Luo*†

*Neurosciences Program, †Department of Biological Sciences, Stanford University, Stanford, California 94305, USA

§Department of Biology and Program in Neuroscience, University of Fribourg, CH-1700 Fribourg, Switzerland

‡These two authors contributed equally to this work

In *Drosophila* and mice, olfactory receptor neurons (ORNs) expressing the same receptors have convergent axonal projections to specific glomerular targets in the antennal lobe/olfactory bulb, creating an odour map in this first olfactory structure of the central nervous system^{1–3}. Projection neurons of the *Drosophila*

antennal lobe send dendrites into glomeruli and axons to higher brain centres⁴, thereby transferring this odour map further into the brain. Here we use the MARCM method⁵ to perform a systematic clonal analysis of projection neurons, allowing us to correlate lineage and birth time of projection neurons with their glomerular choice. We demonstrate that projection neurons are prespecified by lineage and birth order to form a synapse with specific incoming ORN axons, and therefore to carry specific olfactory information. This prespecification could be used to hardwire the fly's olfactory system, enabling stereotyped behavioural responses to odourants. Developmental studies lead us to hypothesize that recognition molecules ensure reciprocally specific connections of ORNs and projection neurons. These studies also imply a previously unanticipated role for precise dendritic targeting by postsynaptic neurons in determining connection specificity.

A common process in neural network formation is the establishment of one-to-one corresponding connections between two groups of neurons in two different locations, thereby generating a neural map (Fig. 1d). Three basic mechanisms for the formation of such neural maps can be proposed. In the first two mechanisms (Fig. 1a, b), either input or target neurons are genetically prespecified, whereas neurons of the remaining field are naive until specified by the identity of their partners during the connection process. In the third mechanism (Fig. 1c), input and target neurons are independently specified. Here, we explore this problem in the wiring of the *Drosophila* olfactory system.

The organization of the *Drosophila* peripheral olfactory pathway is very similar to that of mammals (Fig. 2a). About 1,300 ORNs expressing 40–60 different receptors^{2,6,7} project their axons to 40–50 individually identifiable glomeruli of the antennal lobe⁸ (equivalent to the mammalian olfactory bulb⁹). Information leaves the antennal lobe through an estimated 150 projection neurons (equivalent to mammalian mitral/tufted cells), whose cell bodies are located at the periphery of the antennal lobe^{4,10} (Fig. 2b). Projection neurons

project their dendrites to glomeruli and their axons to higher brain centres, including the mushroom bodies and the lateral horn (Fig. 2a–c, see below). As in mice¹, each ORN probably expresses one specific receptor², and the axons of ORNs expressing the same receptors converge at the same morphologically and spatially distinct glomeruli^{2,3}. In mice, ORNs seem to be genetically programmed to project to specific glomeruli, instructed by the receptors that they express¹¹; indeed, this convergence seems to be independent of the presence of the target neurons of the olfactory bulb¹². Although analogous experiments have not been reported in flies, ORNs expressing a particular receptor reside in stereotypic and discrete zones of the antennae and maxillary palps—the fly's olfactory appendages^{2,6,7}. Assuming that ORN cell bodies do not relocate after their axons reach the antennal lobe, it seems probable that their glomerular targets are prespecified. Thus, of the three models for formation of the neural map (Fig. 1), the second

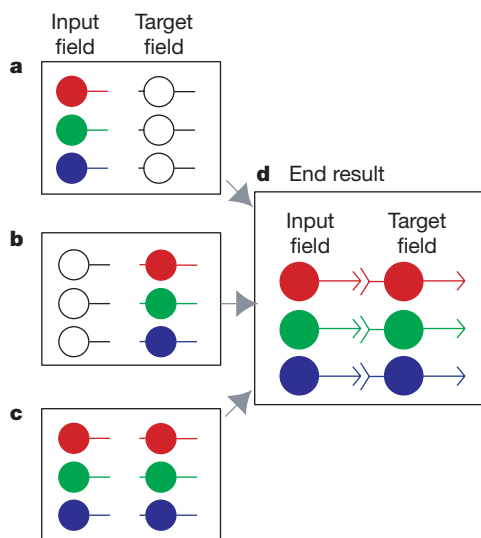


Figure 1 Three mechanisms of establishing a neural map between two classes of neurons in different fields (**d**). **a**, Neurons in the input field are prespecified. Neurons in the target field acquire their identity from incoming neurons of the input field. **b**, Target neurons are prespecified. Input neurons acquire their identity from the target neurons with which they connect. **c**, Input and target neurons are independently specified. Matching colours signify that two neurons will eventually carry the same information, such as activation of a specific odourant receptor. Although we use one-to-one connections for simplicity, a similar logic applies to many-to-one (convergent) or one-to-many (divergent) connections.

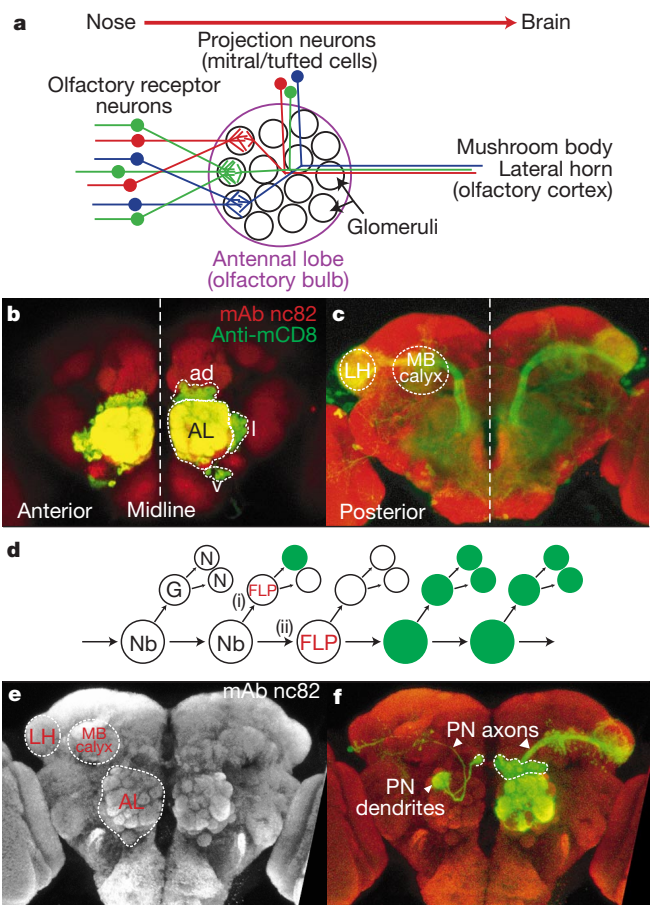


Figure 2 Organization of the antennal lobe. **a**, Schematic of the *Drosophila* olfactory system, with mammalian counterparts in parentheses. Particular colours represent ORNs expressing particular receptors and the projection neurons that form synapses with these ORNs. **b, c**, GAL4-GH146 drives marker (mouse CD8-GFP, green) expression in most of the projection neurons, counterstained with a general neuropil marker nc82 (red). Anterior confocal sections (**b**) show anterodorsal (ad), lateral (l) and ventral (v) cell-body clusters and their dendrites in the antennal lobe (AL); posterior sections (**c**) show axon tracts and their branches in the mushroom body (MB) and lateral horn (LH). mAb, monoclonal antibody. **d**, With MARCM⁵ one can generate positively labelled single-cell clones (i) or neuroblast clones containing all neurons from a neuroblast lineage born after the mitotic recombination event (ii). Nb, neuroblast; G, ganglion mother cell; N, (postmitotic) neuron. **e, f**, Single-cell (left hemisphere) and neuroblast (right) projection neuron clones visualized by mouse CD8-GFP marker (green) counterstained with nc82 (red, shown alone in **e**). The cell bodies of each clone are surrounded by dotted lines. These and all subsequent images are anterior views with dorsal side up. PN, projection neuron.

model seems unlikely in both mice and *Drosophila*. We wanted to distinguish whether *Drosophila* projection neurons are specified by virtue of their connection with ORNs (Fig. 1a) or are independently specified (Fig. 1c).

The MARCM (mosaic analysis with a repressible cell marker) system⁵ can be used to determine neuronal lineage and the projection patterns of individual neurons¹³. A typical neuroblast in the *Drosophila* brain undergoes asymmetric division to regenerate a new neuroblast and a ganglion mother cell, which divides once more to generate two postmitotic neurons. Using MARCM, one can generate positively-labelled single-cell clones as well as neuroblast clones (Fig. 2d). By controlling the timing of mitotic recombination using heat-shock-induced FLP recombinase, one can produce labelled clones of cells born at different developmental times. To study projection neurons of the antennal lobe, we made use of a GAL4 line, GAL4-GH146 (ref. 14), which drives marker expression in a large subset of projection neurons (approximately 90). By crossing GH146 with a membrane marker, UAS-mouse CD8-green fluorescent protein (GFP)⁵, we can visualize the cell body and dendrites of projection neurons in the antennal lobe in the anterior part of the brain (Fig. 2b), as well as their axonal projections in the posterior part of the brain (Fig. 2c). When we apply the MARCM technique using GAL4-GH146, we can selectively visualize subsets of these projection neurons as either neuroblast clones or single-cell clones (Fig. 2f).

Systematic clonal analysis revealed that GH146-positive projection neurons (to which we refer hereafter as projection neurons) are derived from three neuroblasts: an anterodorsal, a lateral and a

ventral neuroblast, corresponding to the three groups of cell body outlined in Fig. 2b. When neuroblast clones are induced in the early embryo and then examined in adults, the anterodorsal, lateral and ventral neuroblasts give rise to approximately 50, 35 and 6 projection neurons, respectively. These three numbers correspond well to the number of projection neurons present in the three GH146-positive cell groups (Fig. 2b). As we cannot induce any clones by applying heat shock after puparium formation (APF), and neuroblast clones generated in late larvae contain 3–5 cells, we infer that all projection neurons are born well before the arrival of pioneering adult ORN axons in the antennal lobe around 20–24 h APF¹⁵. We focused our subsequent analyses on anterodorsal projection neurons and lateral projection neurons as most of these neurons have uniglomerular dendritic projections (see Fig. 2f, Fig. 4b), whereas some ventral projection neurons have diffuse dendritic arborizations, and all project by means of a different path to the higher brain centres, bypassing the mushroom bodies (our own unpublished data).

When glomerular projections of neuroblast clones generated in early larvae were examined, we found that anterodorsal and lateral neuroblast clones appear to innervate stereotypical, intercalated but non-overlapping glomeruli. Figure 3a shows a single confocal section of two independently generated anterodorsal neuroblast clones, revealing almost identical glomerular projections. By contrast, an anterodorsal neuroblast clone and a lateral neuroblast clone examined at the same depth project to complementary glomeruli (Fig. 3b). Figure 3c summarizes the ‘landmark’ glomeruli (see Methods) that are innervated by anterodorsal projection neurons (green) or lateral projection neurons (red). In the 54 anterodorsal neuroblast and 25 lateral neuroblast clones we examined, we found no exception to this rule, despite the fact that there is no obvious relationship between the positions of projection neuron cell bodies and their glomeruli⁴. These observations indicate that the neuroblast from which a projection neuron is derived restricts its glomerular choice and consequently the subset of olfactory information that it can carry further into the brain.

We next asked whether projection neurons are further specified within a neuroblast lineage. Because labelled, single-cell MARCM clones are born shortly after heat-shock induction of mitotic recombination¹³, we could test whether projection neurons born during specific developmental periods would project to specific glomeruli by using the time of heat shock as a variable (see Methods). We found that anterodorsal single-cell projection neuron clones with particular glomerular projections were generated within restricted and characteristic developmental windows (Fig. 4a, b). Notably, single-cell clones induced by early larval heat shock (0–36 h) exclusively produced projection neurons projecting to glomerulus DL1.

Because individual larvae develop at different rates, and FLP recombinase can persist for some time after heat-shock induction, single-cell clone analysis cannot distinguish unequivocally the birth order of projection neurons that are born immediately after each other (Fig. 4a). We therefore took a complementary approach in which we examined multicellular neuroblast clones generated at different developmental periods, and determined whether they included certain landmark glomeruli. If projection neurons innervating different glomeruli are produced in a defined sequence, then multicellular neuroblast clones (Fig. 2d) induced at progressively later times during development should innervate a subset of the glomeruli in neuroblast clones generated at earlier times. Eventually the last-born, smallest clones should contain projection neurons innervating only one glomerulus. Such a nested set is exactly what we observed when anterodorsal neuroblast clones were scored for the presence or absence of projection neurons innervating ten landmark glomeruli (Fig. 5). We could therefore infer an ordered birth sequence of projection neurons (VA2, DL1, DC2, D, VA3, VA1d, VM7, VM2, DM6, VA1lm) from the 54 clones analysed. We

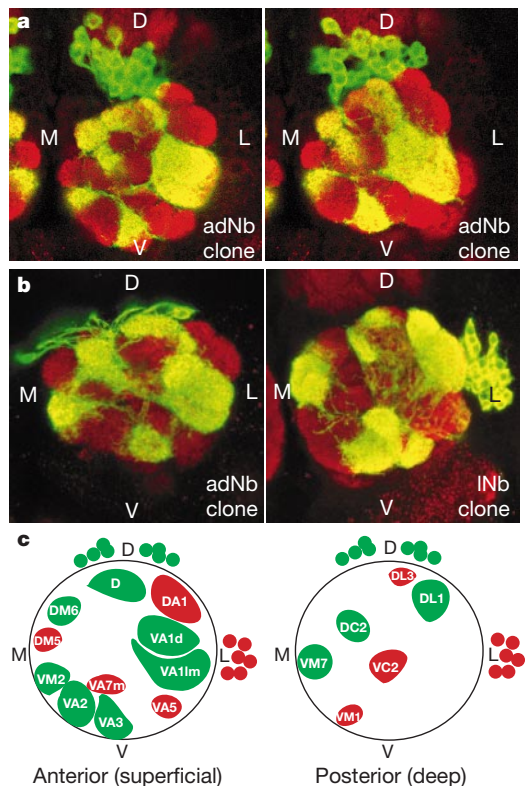


Figure 3 Dorsal and lateral neuroblast clones contain projection neurons with stereotypical and complementary glomerular projections. **a**, Single, confocal sections of two independent anterodorsal neuroblast (adNb) clones taken at similar depths. **b**, Single, confocal sections of an anterodorsal neuroblast and a lateral neuroblast (lNb) clone taken at similar depths. **c**, Schematic of landmark glomeruli derived from anterodorsal neuroblast (green) and lateral neuroblast (red) in the anterior (superficial) or posterior (deep) sections of the antennal lobe. D, dorsal; V, ventral; M, medial; L, lateral.

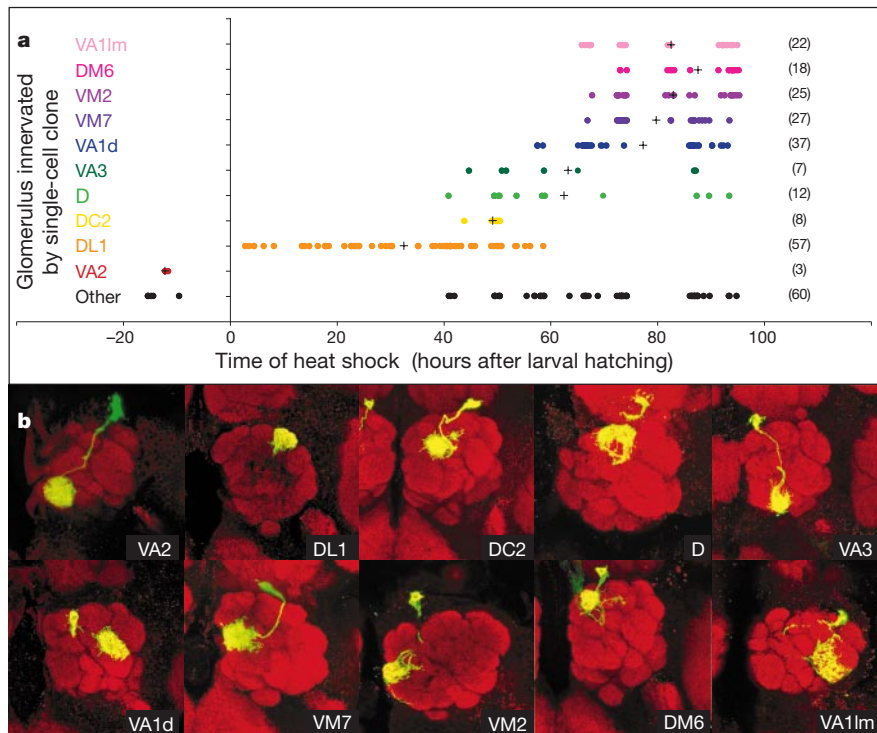


Figure 4 Single-cell clone analysis. **a**, Glomerular identity plotted against time of heat-shock induction for 276 single-cell clones from the anterodorsal neuroblast lineage. Each dot represents a single clone, and crosses represent the mean heat-shock time for a

particular glomerular class. Numbers in parentheses represent the total single-cell clones per glomerular class. **b**, Representative images of the ten landmark single-cell clone classes.

did not find a neuroblast clone in which projection neurons projecting to a particular glomerulus were altered from this order; for example, neuroblast clones containing projection neurons projecting to VM7 always additionally contained all three of the later-born types of projection neuron, VM2, DM6 and VA1Im. As, on average, about three projection neurons innervate each glomerulus, the fact that we can infer an order implies that projection neurons innervating a common glomerulus are likely to be born at a similar time. Together with the single-cell clone analysis (Fig. 4), we conclude that, at least for these ten glomeruli, there is a strict order of generation of projection neurons that can predict future glomerular targets.

How can the birth time of a projection neuron predict which glomerulus it will eventually innervate? One possibility is that the ordered generation of projection neurons could result in the ordered differentiation of their dendrites, and that temporally ordered availability of proto-glomeruli for innervation restricts projection neurons born at a certain time to a particular glomerulus. However, we found that at around 22 h APF, when pioneering ORN axons just start to invade the antennal lobe¹⁵, projection neurons born at different times had similar dendritic differentiation statuses, having already initiated their dendritic branches in the vicinity of the antennal lobe region. The axons of the projection neurons had already reached the mushroom body and the lateral

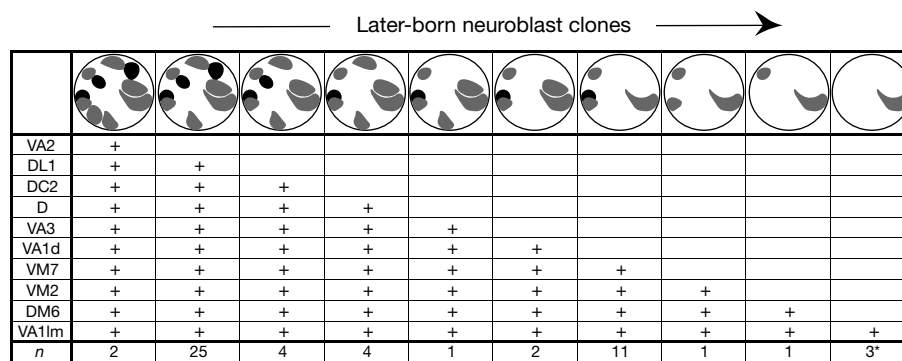


Figure 5 Ordered generation of projection neurons derived from neuroblast clone analysis. Anterodorsal neuroblast clones were scored for the presence (+) or absence of landmark glomeruli; all 54 clones fell into one of ten classes (top). Although we did not use the time of clone induction to deduce order, larger clones were generated from earlier

heat shocks (as represented by the arrow) with few exceptions. Darker glomeruli represent those in deeper sections. Asterisk, these clones are neuroblast rather than single-cell clones because they contain 3–5 projection neuron cell bodies.

horn (see Supplementary Information Fig. 1). These observations argue against the hypothesis of differentiation timing. We instead favour the hypothesis that individual projection neurons and ORNs are independently specified to carry molecular signals that allow them to recognize either each other or a common set of cues located at the developing antennal lobe (Fig. 1c). Although it is assumed that stereotyped ORN axon projections^{2,3} depend on a guidance map in the developing antennal lobe, our results imply that such cues may also be used for precise dendritic targeting of projection neurons, or that projection neuron dendrites actively participate in creating the guidance map.

Independent pre-patterning of input and target fields has been demonstrated in the formation of vertebrate retinotectal projections along the anterior–posterior axis^{16,17}, and even implicated in the development of ocular dominance columns¹⁸. In both systems, activity-dependent processes have important roles in refining the coarse map at the level of the single cell^{19,20}. We show here the independent specification of projection neurons at the single-cell level—matching the precision of the ORN identities. These experiments support the importance of independent specification (Fig. 1c) in formation of the neural map. Moreover, as no obvious logic correlates cell body position of the projection neuron, birth time and the location of the glomerular projection, simple molecular gradient/counter-gradient models as used for axon guidance in the retinotectal system^{16,17} are unlikely to suffice. Instead, we propose that dendrites of projection neurons use a combination of recognition molecules specific to each eventual glomerulus; mechanisms that generate a complex repertoire of cell-surface molecules have recently been described^{21,22}. Furthermore, our study uncovers an elegant mechanism for specifying different projection neurons: the precisely ordered generation by a single neuroblast of a large number of distinct neurons. We are in the process of determining whether a timer mechanism intrinsic to the neuroblast, cues from neighbouring cells at the time of birth, or a combination of such mechanisms^{23–25} are used, perhaps to specify the expression of recognition molecules.

Given the similarities in organization of the *Drosophila* and mammalian peripheral olfactory systems, it will be of great interest to test whether and to what extent the mitral/tufted cells in the mammalian olfactory system are independently specified. It is conceivable that the information used to pattern the olfactory bulb for ORN axon targeting could be used to prespecify mitral/tufted cells, thereby coordinating their dendritic targets in the olfactory bulb and axonal projections in higher brain centres. Such prespecification mechanisms may also be used in neural map formation in other parts of the developing brain. □

Methods

Clonal analysis

In the MARCM strategy, a cell marker is under the control of a GAL4-UAS promoter, which is activated by GAL4 and repressed by GAL80 (ref. 5). The *GAL80* transgene is driven by a ubiquitous promoter and placed distal to an FLP-mediated recombination site. Flies heterozygous for the *GAL80* transgene and carrying appropriate *GAL4* and *UAS-marker* transgenes do not normally express the marker owing to inhibition by *GAL80*. Only after FLP-mediated mitotic recombination will the marker be expressed in cells that have lost the *GAL80* transgene and express the *GAL4* transgene. We maintained flies on standard medium at 25 °C. Larvae of the genotype *y w hs-FLP UAS-mCD8-GFP/ (+ or Y); FRT^{G13} tubP-GAL80/FRT^{G13} GAL4-GH146 UAS-mCD8-GFP* were collected over a 2-h period. After appropriate aging, they were given a 1-h heat shock at 37 °C. To verify that clones homozygous for the *FRT^{G13}* and *GAL4-GH146* insertions (both located on chromosome arm 2R) exhibit no abnormalities, we performed control experiments with larvae of the genotype *y w hs-FLP UAS-mCD8-GFP/Y; tubP-GAL80 FRT^{40A}/FRT^{40A} GAL4-GH146 UAS-mCD8-GFP*, and observed no difference in clone composition or neuronal structure.

Immunocytochemistry and imaging

Adult brains were dissected out at least 48-h after eclosion. Fixation and immunocytochemistry were carried out as described¹³ using the following antibodies: rat monoclonal anti-mouse CD8 α -subunit (Caltag), 1:100; mouse monoclonal nc82 (a gift of E. Buchner and

A. Hofbauer), 1:20; mouse monoclonal 1D4 (gift of C. Goodman), 1:20; Alexa-488 conjugated goat anti-rat immunoglobulin- γ (IgG), 1:200; and Alexa-568 conjugated goat anti-mouse IgG, 1:200 (Molecular Probes). Stacks of optical sections, usually at 0.5- μ m spacing, were obtained with a Bio-Rad MRC 1024 laser-scanning confocal microscope, using the Laser Sharp image-collection program, then processed with NIH Image and Adobe Photoshop.

Glomerular analysis

A subset of the previously recognized glomeruli⁸ were selected as landmark glomeruli because we were unambiguously able to recognize them in neuroblast clones. In the anterodorsal neuroblast lineage, projection neurons born in embryonic and larval stages innervate approximately 5 and 13 glomeruli, respectively. For the lateral neuroblast all GH146-positive projection neurons are probably born later than 24 h after larval hatching and innervate approximately 12 glomeruli. We were unable to generate sufficient partial lateral neuroblast clones to determine the order of lateral projection neuron generation, so we restricted the birth order analysis to the anterodorsal neuroblast. Figures 3–5 tabulate information from more than 4,000 brains examined.

Received 3 July; accepted 27 September 2001.

1. Axel, R. The molecular logic of smell. *Sci. Am.* **273**, 154–159 (1995).
2. Vosshall, L. B., Wong, A. M. & Axel, R. An olfactory sensory map in the fly brain. *Cell* **102**, 147–159 (2000).
3. Gao, Q., Yuan, B. & Chess, A. Convergent projections of *Drosophila* olfactory neurons to specific glomeruli in the antennal lobe. *Nature Neurosci.* **3**, 780–785 (2000).
4. Stocker, R. F., Lienhard, M. C., Borst, A. & Fischbach, K.-F. Neuronal architecture of the antennal lobe in *Drosophila melanogaster*. *Cell Tissue Res.* **262**, 9–34 (1990).
5. Lee, T. & Luo, L. Mosaic analysis with a repressible cell marker for studies of gene function in neuronal morphogenesis. *Neuron* **22**, 451–461 (1999).
6. Vosshall, L. B., Amrein, H., Morozov, P. S., Rzhetsky, A. & Axel, R. A Spatial map of olfactory receptor expression in the *Drosophila* antenna. *Cell* **96**, 725–736 (1999).
7. Clyne, P. J. *et al.* A novel family of divergent seven-transmembrane proteins: candidate odorant receptors in *Drosophila*. *Neuron* **22**, 327–338 (1999).
8. Laissue, P. P. *et al.* Three-dimensional reconstruction of the antennal lobe in *Drosophila melanogaster*. *J. Comp. Neurol.* **405**, 543–552 (1999).
9. Hildebrand, J. G. & Shepherd, G. M. Mechanisms of olfactory discrimination: converging evidence for common principles across phyla. *Annu. Rev. Neurosci.* **20**, 595–631 (1997).
10. Stocker, R. F. The organization of the chemosensory system in *Drosophila melanogaster*: a review. *Cell Tissue Res.* **275**, 3–26 (1994).
11. Mombaerts, P. Molecular biology of odorant receptors in vertebrates. *Annu. Rev. Neurosci.* **22**, 487–509 (1999).
12. Bulfone, A. *et al.* An olfactory sensory map develops in the absence of normal projection neurons or GABAergic interneurons. *Neuron* **21**, 1273–1282 (1998).
13. Lee, T., Lee, A. & Luo, L. Development of the *Drosophila* mushroom bodies: sequential generation of three distinct types of neurons from a neuroblast. *Development* **126**, 4065–4076 (1999).
14. Stocker, R. F., Heimbeck, G., Gendre, N. & de Belle, J. S. Neuroblast ablation in *Drosophila* P[GAL4] lines reveals origins of olfactory interneurons. *J. Neurobiol.* **32**, 443–452 (1997).
15. Jhaveri, D., Sen, A. & Rodrigues, V. Mechanisms underlying olfactory neuronal connectivity in *Drosophila*—the atonal lineage organizes the periphery while sensory neurons and glia pattern the olfactory lobe. *Dev. Biol.* **226**, 73–87 (2000).
16. Sperry, R. W. Chemoaffinity in the orderly growth of nerve fiber patterns and connections. *Proc. Natl Acad. Sci. USA* **50**, 703–710 (1963).
17. Flanagan, J. G. & Vanderhaeghen, P. The ephrins and Eph receptors in neural development. *Annu. Rev. Neurosci.* **21**, 309–345 (1998).
18. Crowley, J. C. & Katz, L. C. Early development of ocular dominance columns. *Science* **290**, 1321–1324 (2000).
19. Goodman, C. S. & Shatz, C. J. Developmental mechanisms that generate precise patterns of neuronal connectivity. *Cell* **72**, 77–98 (1993).
20. Katz, L. C. & Shatz, C. J. Synaptic activity and the construction of cortical circuits. *Science* **274**, 1133–1138 (1996).
21. Wu, Q. & Maniatis, T. A striking organization of a large family of human neural cadherin-like cell adhesion genes. *Cell* **97**, 779–790 (1999).
22. Schmucker, D. *et al.* Dscam is an axon guidance receptor exhibiting extraordinary molecular diversity. *Cell* **101**, 671–684 (2000).
23. McConnell, S. K. Strategies for the generation of neuronal diversity in the developing central nervous system. *J. Neurosci.* **15**, 6987–6998 (1995).
24. Edlund, T. & Jessell, T. M. Progression from extrinsic to intrinsic signaling in cell fate specification: a view from the nervous system. *Cell* **96**, 211–224 (1999).
25. Ishiki, T., Pearson, B., Holbrook, S. & Doe, C. Q. *Drosophila* neuroblasts sequentially express transcription factors which specify the temporal identity of their neuronal progeny. *Cell* **106**, 511–521 (2001).

Supplementary information is available on Nature's World-Wide Web site (<http://www.nature.com>) or as paper copy from the London editorial office of Nature.

Acknowledgements

We thank members of the Luo laboratory and B. Baker, S. McConnell, W. Newsome, J. Ngai, C. Niell and D. Hoepfner for comments on the manuscript. G.S.X.E.J. and E.C.M. are HHMI pre-doctoral fellows. This work was supported by a Swiss National Funds grant to R.F.S. and NIH grants and a Terman Fellowship to L.L.

Correspondence and requests for materials should be addressed to L.L. (e-mail: lluo@stanford.edu).